PAPER

Check for updates

A wear and heat-resistant hydrophobic fluoride-free coating based on modified nanoparticles and waterborne-modified polyacrylic resin†

Bin Yu, Huicong Liu, [ID] * Haining Chen, [ID] Weiping Li, [ID] Liqun Zhu and Weitao Liang [ID] *

Hydrophobic coatings have attracted extensive research due to their broad application prospects. However, hydrophobic coatings in practical applications are often limited by their insufficient stability and are difficult to be applied on a large scale. In this regard, wear and heat resistance are key aspects that must be considered. In this paper, a method for preparing a robust hydrophobic coating with modified ZrO_2 particles as the core component and modified acrylic resin is proposed. First, γ-aminopropyltriethoxysilane (APTES) was used to silanize ZrO_2 to obtain Si–ZrO_2 nanoparticles, which were grafted with amino groups. Then, the nanoparticles reacted with isocyanates to be grafted with hydrophobic groups. A simple spray method was developed to deposit a hydrophobic (141.8°) coating using the mixture containing the modified nanoparticles and non-fluorinated water-based silicon-modified acrylic resin (WSAR) that was prepared by free radical polymerization. The obtained coating exhibited a rough surface and the particles and resin were closely combined. Compared with pure resin coating, the composite coating exhibited 150% enhancement in wear resistance and it could wear 45 meters at a pressure of 20 kPa. Moreover, the coating could maintain the hydrophobic property even when it lost 70% quality or after it was heated at 390 °C. The thermogravimetric results showed that the temperature could reach 400 °C before the quality of the fluorine-free coating dropped to 90%. In addition, the coating could easily take away graphite or silicon carbide powder under the impact of water droplets, showing excellent self-cleaning performance.

1 Introduction

The hydrophobic phenomenon found in lotus leaves has been extensively studied in recent years. Generally speaking, hydrophobic refers to the water contact angle greater than 90°, while superhydrophobic refers to the water contact angle greater than 150° with a small rolling angle.[1,2] The construction of hydrophobic coatings requires two conditions: one is a certain surface roughness, and the other is low surface energy.[3–7] There are many ways to prepare superhydrophobic films, which can be basically divided into two directions: top-down and bottom-up. Top-down approaches include lithography and template-based techniques[8] and surface plasma treatment.[9,10] Bottom-up approaches mainly involve self-assembly and self-organization.[11–13] Bottom-up approaches include chemical deposition,[14–16] layer-by-layer (LBL) deposition,[14,17] and colloid assembly.[18,19] Thus far, superhydrophobic coatings with water

contact angles of more than 150° or even 170°, have been widely reported.[20,21] However, due to the fragile structure and easy chemical degradation of hydrophobic surfaces, poor mechanical and thermal stability have limited the wide application of hydrophobic surfaces.[22–25]. Thus, preparing hydrophobic coatings with high mechanical and thermal stability is of practical interest.

So far, several coatings with high mechanical and thermal stability have been developed.[25–28]. In these strategies, the resin is often used as a film-forming component and is modified for heat resistance.[29,30] It is noteworthy that the coatings that could maintain hydrophobicity at temperatures above 350 °C often use fluorosilane-modified resins, which utilize the low surface energy and high bond energy of fluorides to obtain hydrophobicity and heat resistance.[31,32] However, long-chain fluorocarbon materials can decompose into per-fluorooctanoic acids, which have been classified as emerging contaminants by the U.S. Environmental Protection Agency.[33–36] However, a few current research on hydrophobic coatings for non-fluorinated systems can withstand more than 350 °C before the mass loss exceeds 10%, so it makes sense to provide a solution for this. In addition, the improvement of wear resistance often relies on the firmness of the substrate itself[37,38] or continuous exposure of

School of Materials Science and Engineering, Beihang University, No. 37 Xueyuan Road, Haidian District, Beijing 100191, People's Republic of China. E-mail: liuhc@buaa.edu.cn; lwt@buaa.edu.cn

† Electronic supplementary information (ESI) available. See DOI: https://doi.org/10.1039/d2ra07237h

repeating structures until worn out[38] or wear-resistant nanoparticles.[39–41] However, relying on the robustness of the substrate itself results in the immediate loss of hydrophobicity when worn, while coatings relying on repetitive structures require high coating thicknesses, which do not meet the requirements of thin coatings for industrial applications. Introducing abrasion resistance particles is also faced with many problems, such as particle selection, compatibility with resins, and methods of grafting modifiers. Moreover, the preparation methods in many papers are too complicated. Such as, surface etching,[28,42] template method,[8] chemical vapor deposition,[39] layer-by-layer assembly[40] etc. These preparation conditions and processes are not realistic for commercial applications. Therefore, there is an urgent need to prepare a scalable and fluorine-free hydrophobic coating that is resistant to wear and high temperature.

Herein, we addressed the above issues in three steps. First, based on the fluorine-free material system composed of the prepared hydrophobic ZrO_2 nanoparticles and water-based silicon-modified acrylate copolymer, a water-based coating was prepared by simply mixing. The reason for choosing ZrO_2 as filler is its excellent wear resistance and high-temperature resistance (melting point 2700 °C), and good compatibility with acrylic resin. Second, a scalable preparation method (spray method) was used to prepare composite coatings with excellent hydrophobic properties (contact angle up to 141.8°). Finally, the robust surface of the composite hydrophobic coating produced excellent wear resistance and thermal stability.

2 Experimental section

2.1 Materials

γ-Aminopropyltriethoxysilane (APTES, 99%), octadecanol (OD, AR), ammonia (AR), butyl acetate (BUA, 99%) were purchased from Aladdin Reagent (Shanghai) Co., Ltd. Nano-zirconia (99.99%), butyl acrylate (BA), purchased from MacLin Reagent Co., Ltd. Benzoyl peroxide (BPO, 75%) was purchased from Adamas reagent (Shanghai). N-Butanol, vinyltriethoxysilane (VTES, 98%), acrylic acid (AA, 99%), butyl acrylate (BA, 99%), dichloromethane (chromatographic grade), dibutyltin dilaurate (DBTDL, 95%), isophorone diisocyanate (IPDI, 99%), 2-hydroxyethyl methacrylate (HEMA, 96%), styrene (ST, 99.5%) were purchased from Innochem Reagent (Beijing) Co., Ltd. All chemicals were used without further purification.

2.2 Preparation of IPDI-grafted long-chain aliphatic alcohol-modified silanized-ZrO_2 particles (Si–ZrO_2–IPDI@OD)

2.2.1 Preparation of silane ZrO_2 particles (Si–ZrO_2) by condensation. Si–ZrO_2 particles were prepared by the co-condensation of APTES. A certain amount of ZrO_2 nanoparticles and APTES were added into a four-necked flask with a condensing tube, and the molar ratio of ZrO_2 : APTES was 1 : 0.55. Then, a small amount of ammonia and a certain amount of ethanol were added and heated at 75 °C for 3 h. Finally, after cooling, centrifugal washing, and drying, Si–ZrO_2 nanoparticles were obtained.

2.2.2 Preparation of surface hydrophobic modifier (IPDI@OD). Since single long-chain alcohols cannot be directly grafted onto Si–ZrO_2 nanoparticles, NCO-groups on IPDI were used to graft with them, and then to graft with the particles. The processes were as follows: a certain amount of IPDI and BUA was added into a four-neck flask, and the temperature was raised to 70 °C under stirring conditions. Then, the mixture of OD and BUA was added, and the molar ratio of IPDI : OD was 2 : 1. After the heat preservation reaction for 2 hours, followed by cooling discharge, a clear surface hydrophobic modifier was obtained.

2.2.3 Preparation of hydrophobically-silanized ZrO_2 particles (Si–ZrO_2–IPDI@OD). The Si–ZrO_2 obtained in step 1 was dispersed in BUA and ultrasonicated for a period of time. Then, it was poured into a four-neck flask and heated to 75 °C. After stirring, a small amount of DBTDL was added. Then, the IPDI@OD obtained in step 2 was slowly dropped into the flask, the ratio of Si–ZrO_2 : IPDI@OD was 2 : 1, and the reaction time was 24 h. Subsequently, it was cooled and washed three times with BUA centrifugation. After drying, Si–ZrO_2–IPDI@OD was obtained.

2.3 Synthesis of water-soluble silicone-modified acrylic resin (WSAR)

Waterborne silicon to acrylic resin was synthesized using free radical polymerization (Fig. 2). With n-butanol as a solvent, 1/2 of the amount was added to the flask and heated to its boiling point by condensation reflux. The monomer is mixed according to a certain proportion, adding BPO, 1/2 solvent left and then slowly drop into the flask, at the end of the drop reaction for 5 h. After cooling, the transparent yellow resin was obtained. After cooling to room temperature, small amounts of ammonia and deionized water were added to complete the water-based
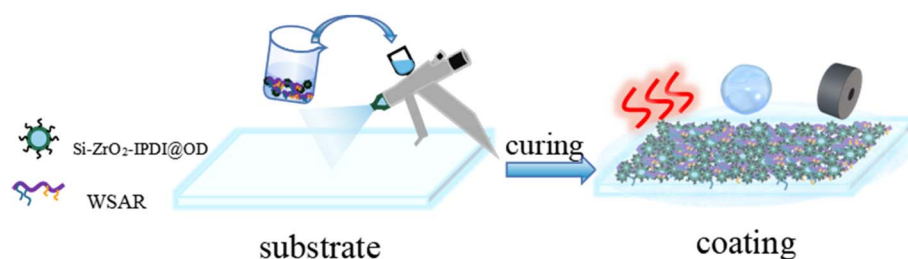

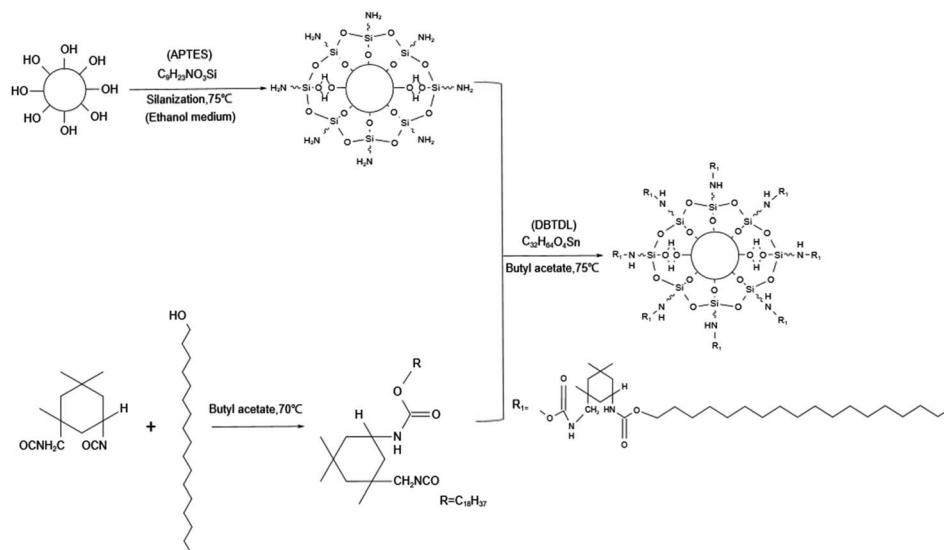Fig. 1 Schematic diagram of the coating preparation.

Fig. 2 Si–ZrO$_2$–IPDI@OD preparation process.

activation. Two different proportions of WSAR (Tables S1 and S2†) were prepared by orthogonal experiment, named ZJ1 best and ZJ2 best.

2.4 Preparation of WSAR/Si–ZrO$_2$–IPDI@OD coatings

WSAR/Si–ZrO$_2$–IPDI@OD coatings were prepared by the spraying method (Fig. 1). The prepared WSAR and Si–ZrO$_2$–IPDI@OD particles were mixed, and a certain amount of CH$_2$Cl$_2$ was added as the solvent to make wt%$_{particles}$ = 5%. The substrate was directly sprayed with a spray gun, and then the substrate was dried and cured to obtain a uniform coating.

2.5 Characterization

The surface morphology of the coating was observed using the SEM JSM7500 instrument (JEOL, Japan). The samples were sprayed with gold before observation. The TEM test was
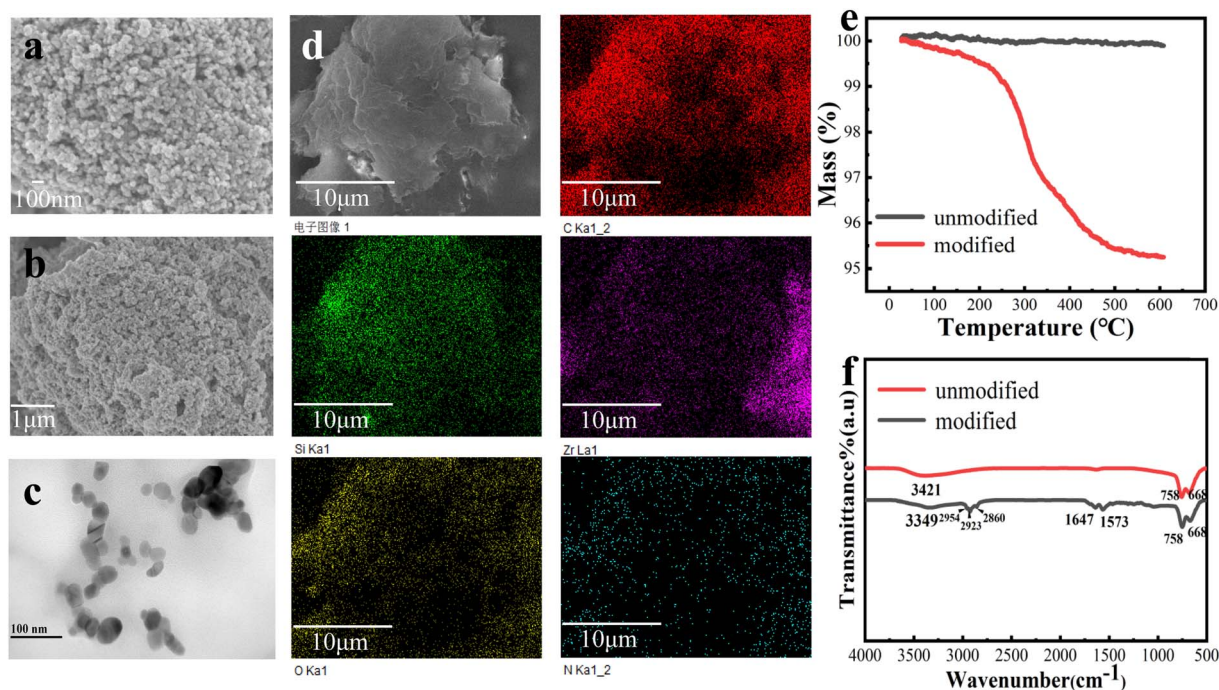

Fig. 3 Characterization of WSAR/Si–ZrO$_2$–IPDI@OD particles. (a) and (b) SEM images of modified particles. Magnification: (a) ×50 000 (b) ×20 000 (c) TEM image of particles. (d) EDS spectra of ZJ1 best-particles 10 : 1. (e) TG curves of particles before and after modification. (f) FTIR spectra of particles before and after modification.

operated on JEM-2100 and the coating was diluted twenty-fold and painted on Cu mesh. The surface roughness of the coating was tested using an atomic force microscope (Veeco DI, USA the material of the cantilever was Si, the spring constant was 40 N m^{-1} and the frequency was 300 kHz). The chemical structures of the resin and modified particles were characterized using infrared spectra with a Fourier-transform infrared spectrum analyzer (FT-IR, Thermo Nicolet AVATAR, Nicolet 6700, USA). Thermogravimetric analysis was performed using the STA-449F3 (NETZSCH-Gerätebau GmbH, Germany) instrument. The method used for the measurement of the static water contact angle was the sessile drop method, operated on a KRÜSS DSA-10 instrument (KRÜSS, Germany). Three different point measurements were taken for each sample. The volume of an individual droplet was 5 μL.

The instrument used for the friction and wear experiments was LC-802B (DONGGUAN LICHUAN EQUIPMENT CO., LTD, China). The experimental principle was that two rollers attached to the 600 grit sandpaper (replace every ten turns) rotate on the substrate, each roller weighs 300 g, and the mass loss of the coating was recorded after every 10 turns. The worn area by the machine was fixed, and the schematic diagram and the quality calculation formula of the worn area are shown in Fig. S3.† The contact area between the roller and the sample during friction was 1.5 cm^2, which means the pressure of the roller on the sample was 20 kPa. The circumference of the roller was 10 cm.

The instrument used for the heat resistance test was a muffle furnace. Thermal stability experiments were performed by gradually heating the samples until they lost their hydrophobicity. After each heating step, the samples were tested for CA value. If the hydrophobicity was not lost, the temperature value was set to 10 °C higher than before until the sample lost the

hydrophobicity. The holding time at the highest temperature was 10 min each time.

3 Results and discussion

3.1 Si–ZrO$_2$–IPDI@OD particles

Fig. 3a and b show the SEM images of the particles. As indicated, the particle size is about 30–50 nm, which was further confirmed from the TEM image (Fig. 3c). The elemental mapping in Fig. 3d shows that there are C, O, N, Si, and Zr, which proves that the modification of particles was successful. Fig. 3e is the thermogravimetric curves of the particles before and after modification. The unmodified particles did not show obvious mass loss in the temperature range. In contrast, though the mass loss of the modified particles was less than 1% before 300 °C, they lost about 5% mass at 300–600 °C, which indicated that the material grafted on the particle surface was decomposed. Therefore, TG results also proved the successful grafting of the particles. FT-IR spectra in Fig. 3f shows that the Zr–O–Zr characteristic absorption peak of ZrO$_2$ is at 668 cm^{-1},[28] and the broad peaks at 3421 cm^{-1} and 3349 cm^{-1} of the unmodified spectrum represented the stretching vibration absorption peaks of Zr–OH and –OH in Si–OH. The modified particles showed Si–OH and N–H bonds due to the APTES silylation reaction, so their peak positions are offset compared with the spectrum of the unmodified particles, which proved that the silylation reaction was successful. The peaks at 2954 cm^{-1}, 2923 cm^{-1}, and 2860 cm^{-1} represented the symmetric stretching vibration absorption peak of –CH$_3$ and the asymmetric stretching vibration absorption peak of –CH$_2$, respectively. The vibration at 1647 cm^{-1} corresponds to the carbonyl group on IPDI, while the peak at 1573 cm^{-1} represents the C–N bond vibration on
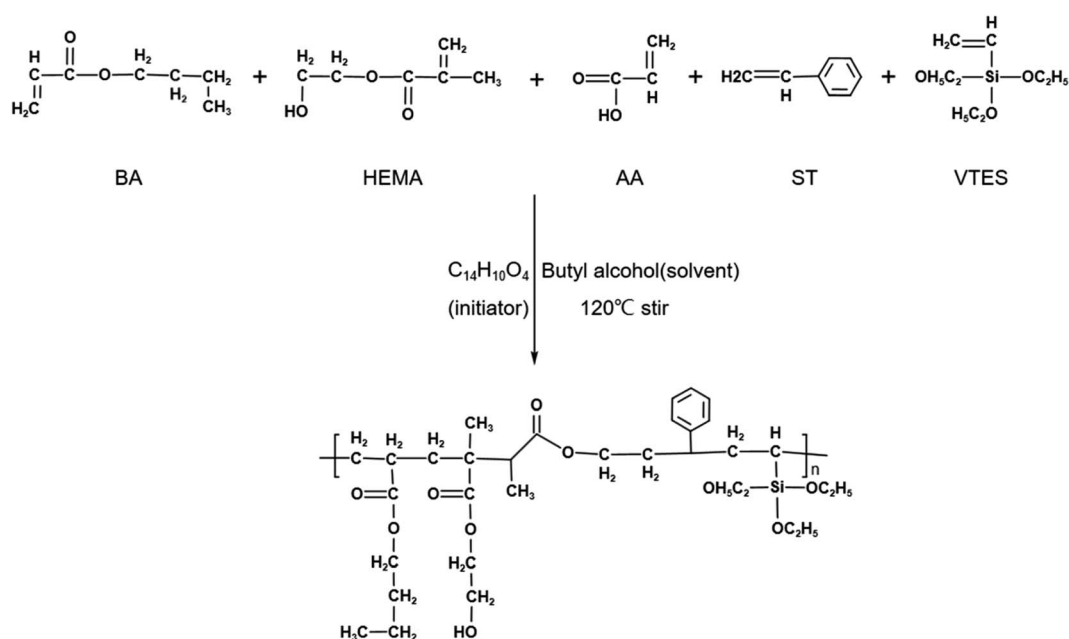

Fig. 4 WSAR preparation process.

surfactant. These results indicate that the surface modifier was successfully grafted onto the particles.

3.2 WSAR/Si–ZrO$_2$–IPDI@OD coating

Fig. 4 shows the process of synthesizing WSAR, which uses radical polymerization. It was designed with the following idea: the composition of acrylic resins includes soft monomers, hard monomers, and functional monomers. Here, BA was selected as a soft monomer, its long carbon chain provided low surface energy for the resin, ST as a hard monomer to improve the ethanol resistance of the resin, AA, and HEMA as functional monomers, and the carboxyl group of AA and the hydroxyl group of HEMA provided functional groups for crosslinking. In addition, the carboxyl group of AA could improve the adhesion of the substrate of the resin. VTES will undergo a hydrolysis reaction to obtain silicon hydroxyl groups in an alkaline alcohol water environment, so during the formation of the coating, not only the crosslinking reaction of silicon hydroxyl groups between the resins will occur, but also the condensation reaction between resin silicon hydroxyl groups and zirconium hydroxyl groups on the surface of nano-ZrO$_2$ will occur at the same time, making the coating stronger.

After synthesizing WSAR, it was first detected by gel permeation chromatography (GPC). Fig. 5 and Table 1 show the test results. In Fig. 5a are GPC spectra of ZJ1 best and ZJ2 best. Fig. 5b and c are the molecular weight and cumulative molecular weight distribution curves of ZJ1 best and ZJ2 best, respectively. Table 1 lists the detailed data. It can be seen that the M_n and M_w of ZJ1 best are greater than those of ZJ2 best, indicating that the molecular weight of ZJ1 best is greater than ZJ2 best, but the polydispersity index of ZJ1 best is 4.4, which is greater than 2.1 of ZJ2 best. In Fig. 5a, the time when the peak of ZJ1 best appeared is earlier than that of ZJ2 best, indicating that its molecular weight is larger, which can also be seen in Fig. 5b and c. In Fig. 5b, the distribution curve of ZJ1 best has two peaks, the first peak has a wide distribution range, and the molecular weight from 42 500 to 52 500 occupies about 54% of the mass. The second peak is very narrow, and the molecular weight from 53 500 to 56 000 occupies about 18% of the mass, so the polydispersity index of ZJ1 best is relatively large. In Fig. 5c, ZJ2 best has only one peak, and the molecular weight from 40 000 to 48 000 occupies about 70% of the mass, so the polydispersity index of ZJ2 best is small.

Table 1 The molecular weight and its distribution of the amount of ZJ1 best and ZJ2 best

	M_n	M_w	M_z	M_{z+1}	M_w/M_n	M_z/M_w
ZJ1 best	28 839	126 150	263 836	347 202	4.4	2.1
ZJ2 best	15 717	32 998	56 580	81 336	2.1	1.7

Fig. 6a is the FT-IR spectra of resins and coatings. The peaks at 1730 cm^{-1} and 1160 cm^{-1} appearing in both spectra could be indexed to the stretching absorption of C=O, and Si–O in acrylic resin, respectively. The peak at 1470 cm^{-1} corresponds to the C=C stretching resonance of the benzene ring on the ST. The absorption peaks at 2960 cm^{-1} and 2870 cm^{-1} are consistent with the stretching vibration peaks of C–H, while the absorption peak at 750 cm^{-1} represents Zr–O–Zr. Therefore, the FT-IR spectra demonstrated that the coating contained both resin and modified particles. Fig. 6b shows the water contact angles and sliding angles of ZJ1 best, ZJ2 best, and their coatings with different ratios of particles. It can be seen that the contact angle and sliding angle of ZJ1 best are better than those of ZJ2 best, but their data are almost the same after the particles are added, which reflects that the hydrophobic ability of the coating is mainly provided by particles. After the particles are added, the contact angle can be greater than 140°, and the sliding angle can be as low as about 5°. After 1 : 10, the changes in contact angle and sliding angle are not obvious. The water droplet rolling on the coating surface is shown in Fig. S5.† It can be found that the water droplets roll off the coating within about 0.1 s. Fig. 6c and e are the top-view SEM images of the ZJ1 best-1 : 1 coating. In Fig. 6c, both exposed particles and wrapped particles can be seen, indicating that particles and resin have good compatibility. Fig. 6d and f are similar to the former. Fig. 6e and f have great differences in coating roughness, which is due to the different particle content. It could be concluded that the higher particle content could lead to the higher roughness of the coating.

3.3 Friction resistance of WSAR/Si–ZrO$_2$–IPDI@OD coating

The wear resistance of the coatings was evaluated by linearly fitting the data obtained by a wear-weighing method (see Fig. S3†). The fitting results of all the wear tests are shown in Table S3.† ZJ1 best and ZJ2 best represent the coatings with the
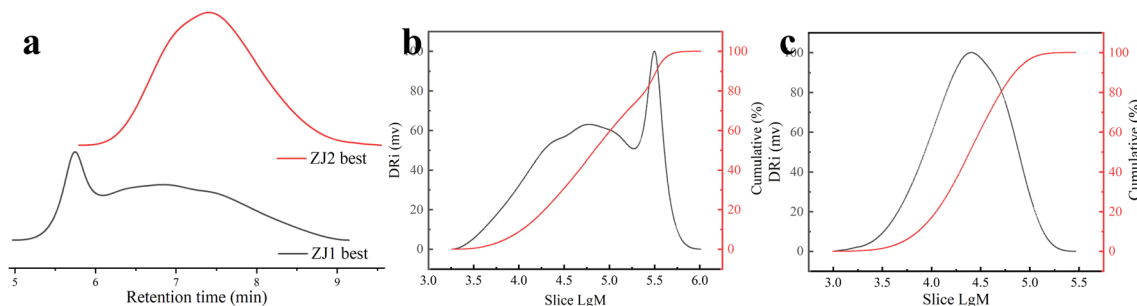

Fig. 5 (a) GPC chromatograms of ZJ1 best and ZJ2 best. (b) Molecular weight and cumulative weight distribution curve of ZJ1 best. (c) Molecular weight and cumulative weight distribution curve of ZJ2 best.
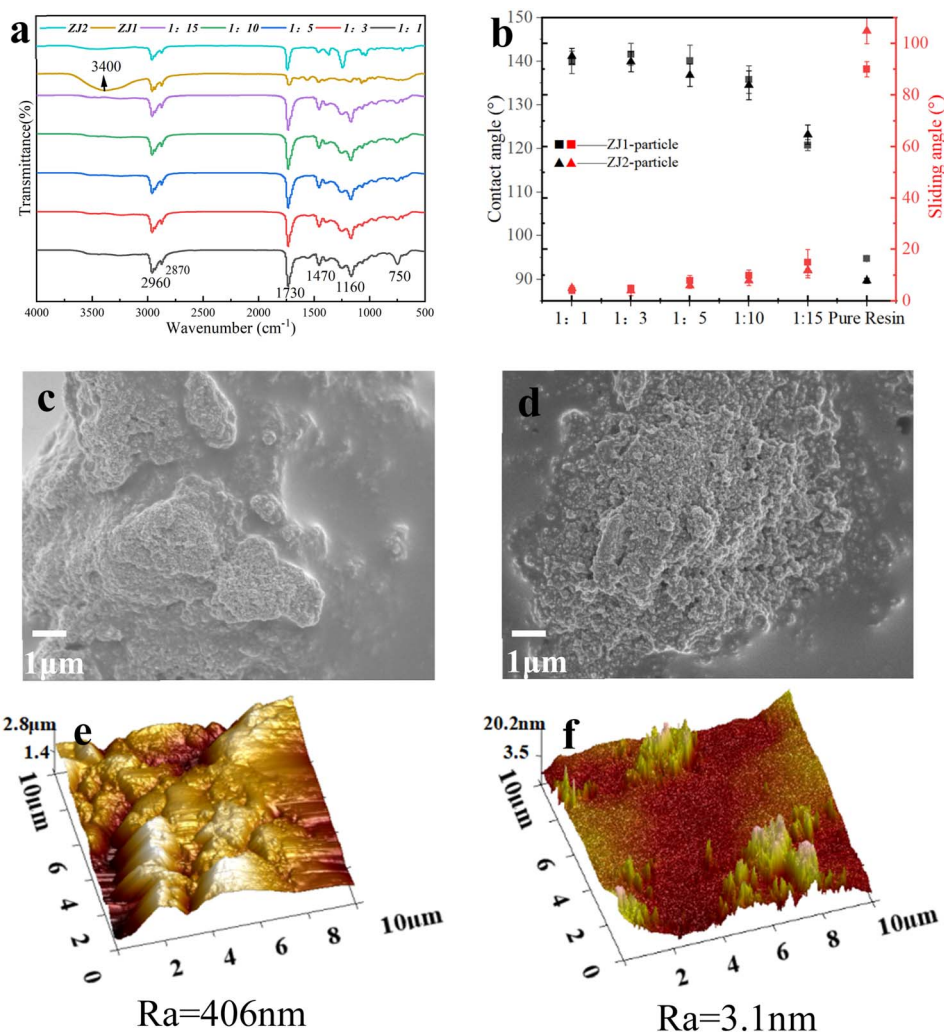
Fig. 6 (a) FT-IR spectra of coatings mixed with different proportions of particles. (b) Contact and sliding angle plots of ZJ1 best coatings mixed with different proportions of particles. (c) and (e) SEM and AFM of ZJ1 best-particle 1 : 1. Magnification: (c) ×10 000. (d) and (f) SEM and AFM of ZJ2 best-particle 15 : 1. Magnification: (d) ×10 000.

best wear performance in the two orthogonal experiments (shown in Fig. S1 and S2†), respectively. The "*a*" in the curve "*y* = *ax* + *b*" represents the quality of the coating lost after each wear cycle. The lower the absolute value of "*a*" is, the more wear-resistant the coating is. Fig. 7a compares the wear resistance of ZJ1 best and ZJ2 best. According to the fitting results, the "*a*" value of ZJ2 best is close to twice that of ZJ1 best, indicating that ZJ1 best's wear resistance is better than ZJ2 best. The wear resistance of ZJ1 best and ZJ2 best particle coatings with different doping ratios are presented in Fig. 7(b–d) and (f–h), respectively. In order to make the experiment data more objective, the experiments of ZJ1 best and ZJ2 best coatings were repeated twice.

As indicated in Fig. 7b–d, the wear resistance of ZJ1 best-particle coating showed a certain regularity, except for the 1 : 5 group, the wear resistance of other groups decreased with the increase of particle content, and the wear resistance was 1 : 5, 1 : 15, 1 : 10, 1 : 3, 1 : 1 from high to low. This phenomenon may occur because the effect of the addition of particles on the

coating is two-sided, as shown in Fig. 7b. In Fig. 7b, the wear resistance of 1 : 5, 1 : 15 and 1 : 10 is better than that of ZJ1 best, while the wear resistance of the 1 : 3 and 1 : 1 groups is weaker than that of ZJ1 best. The decrease in wear resistance is due to the decrease in the toughness of the coating because of the increase in particles. In a frictional environment, the higher the particle content, the more brittle the coating is and the more likely to come off the surface. However, the increased wear resistance of the coating by particles results in optimal particle doping of the coating. Therefore, for ZJ1 best, the optimal amount of particles added is 1 : 5. As for why the wear resistance of the coating has not been rising before the addition of 1 : 5, that is, why the wear resistance of 1 : 15 is higher than 1 : 10. This is because when there are fewer particles, such as 1 : 15, the resin is the main part that bears the wear, and the particles play an auxiliary role. When there are more particles, such as 1 : 5, the particles are the main part that bears the wear, and the resin plays an auxiliary role. When there are too many particles, such as 1 : 3 and 1 : 1, it will destroy the coordination of the coating
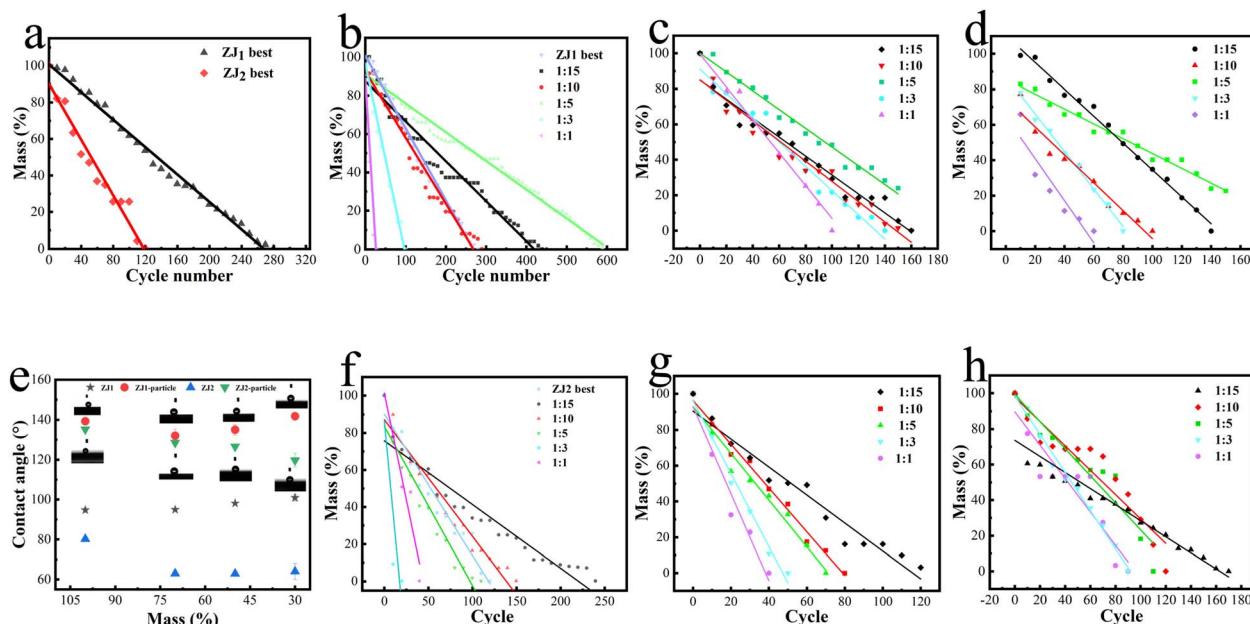
Fig. 7 (a) Comparison of wear resistance between ZJ1 best and ZJ2 best. (b–d) Repeated testing for abrasion resistance of ZJ1 best mixed with different proportions of particles. (e) Changes of contact angle during wear. (f–h) Repeated testing for abrasion resistance of ZJ2 best mixed with different proportions of particles.

and reduce the wear resistance. Therefore, in this series of experiments, 1 : 10 is between the two states of 1 : 15 and 1 : 5, so, understandably, the wear resistance is lower than 1 : 15. In a word, in this experiment, the sample with the best wear resistance was from the 1 : 5 group. The best performance in wear resistance in this series of experiments was 1 : 5, as shown in Fig. 7b, which was 150% higher than that of ZJ1 best.

As indicated in Fig. 7f–h, the wear resistance of each coating increases with the increase of particle content in the three ratios of 1 : 15, 1 : 10, and 1 : 5, while there is no clear difference in wear resistance between the 1 : 1 and 1 : 3 groups. The reasons for these two phenomena may be: first, in Fig. 7a, it can be seen that the wear resistance of ZJ2 best is not as good as ZJ1 best, so the promotion of wear resistance by particles is more visible in ZJ2 best. Second, after reaching the ratio of 1 : 3, the promotion effect of particles on ZJ2 best has reached the upper limit, and continuing to increase particles can not bring more improvement, so the wear resistance of the 1 : 1 and 1 : 3 groups is not determined. The biggest improvement in wear resistance in this series of experiments was in the 1 : 15 group, as shown in Fig. 7f, which was 124% higher than that of ZJ2 best. As for the reason why the wear resistance of ZJ2 best is not as good as that of ZJ1 best, it may be caused by the difference in the synthesis scheme of the two. In Tables S1 and S2,† it can be seen that a large amount of BA and a small amount of ST were used to synthesize ZJ1 best, while ZJ2 best was the opposite. The long carbon chain of BA is conducive to forming a network entanglement structure to improve wear resistance, while ST's benzene ring occupies space to hinder polymers from winding each other, which is not conducive to improving the wear resistance.

Fig. 7e is the change in the contact angle for different coatings during wear. It can be seen that pure resin coatings like ZJ1

best and ZJ2 best show poor hydrophobic properties. After wear, the contact angle of ZJ2 best decreases rapidly, and ZJ1 best can better maintain hydrophobic ability in wear. Coatings with particles are shown in this figure, their contact angles are greatly improved, and their hydrophobicity is also maintained during wear. The ZJ1 best-particle group shows the best performance, and it still maintains a high hydrophobic angle after losing 70% mass of the coating.

Compared with other reported wear-resistant hydrophobic coatings, a highlight of this work is the clear evaluation of the wear resistance of the coating. This article evaluates the wear resistance of coatings by evaluating the mass lost per wear so that the wear resistance can be converted into specific numbers. In some reports, only the change in the contact angle of the coating is used as an evaluation criterion. In the reports of using sandpaper as a wear medium, 800 mesh or 1000 mesh sandpaper is usually used, the load is generally 1–3 kPa, and the coating can withstand about 1 m of wear.[43–45] In this work, a 600 mesh sandpaper and a 20 kPa load were used for abrasion experiments, and the best-performing sample could wear more than 45 m (1 : 5 sample, as shown in Fig. 6b was 450 turns at 30% mass).

When wear occurs, grain abrasion is the main wear mechanism. Grain abrasion is a material loss caused by the passing of hard particles on the surface. During this period, micro-cutting, micro-fracture, and micro-plowing are often observed.[46] These phenomena can be observed in Fig. 8h and i. The role of the particles in friction can be divided into two points: one is the rolling effect of particles. This rolling effect helps to reduce the friction coefficient during sliding, which thereby reduces shear stress and contact temperature.[47–49] The other is the addition of particles is tightly related to the resin. When friction occurs to the
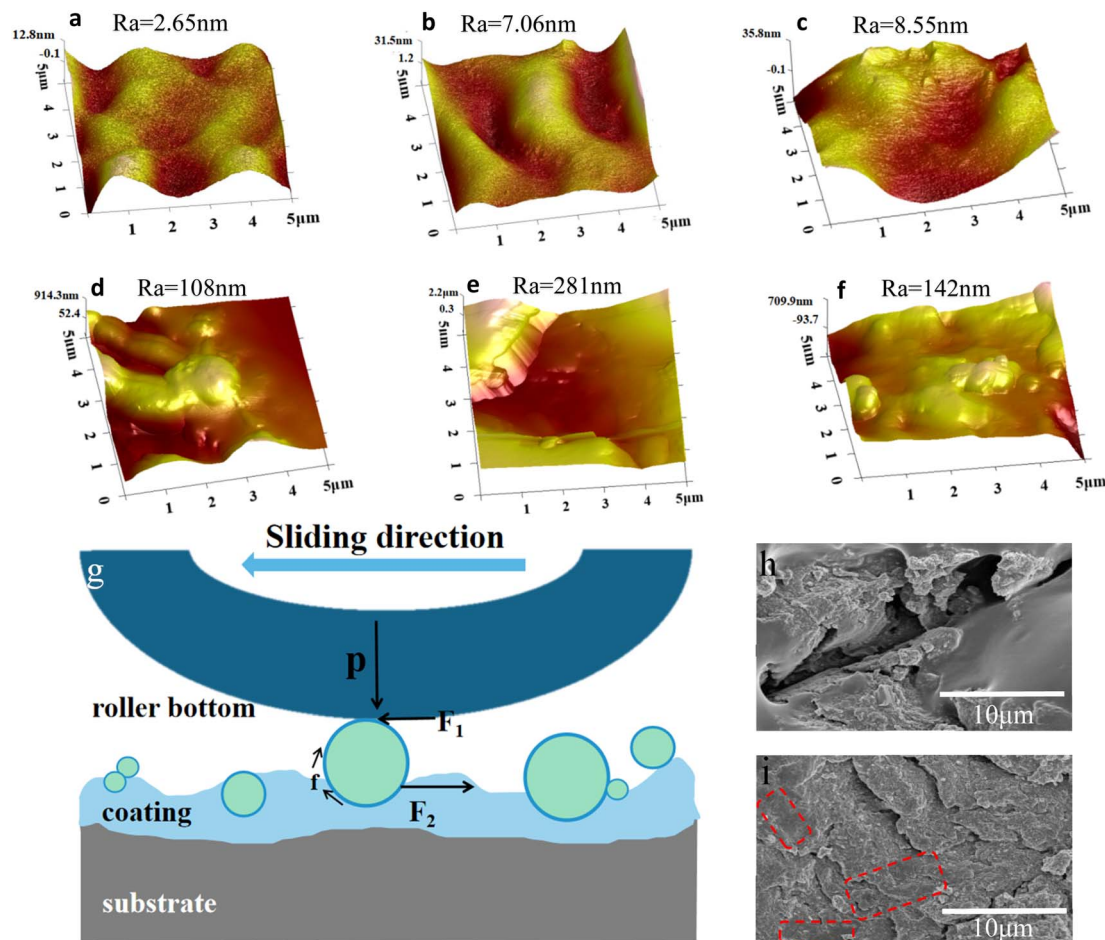
Fig. 8 (a–c) AFM pictures of ZJ1 best-particle coating with different wear degrees. (a) 30% (b) 50% (c) 80% (the mass percentage loss of the worn part of the coating). (d–f) AFM pictures of ZJ2 best-particle coating with different wear degrees. (d) 30% (e) 50% (f) 80%. (g) Particle force analysis diagram. (h and i) SEM of the coating after wear. Magnification: (h) ×5000 (i) ×5000.

particles, the combination of particles and resin matrix will play a blocking role. When the external force exceeds the binding force between particles and resin, friction continues. Fig. 8g is the force analysis of particles in the wear process. In the figure, P represents the pressure of the roller on the particle, F_1 is the friction force of the roller to the particle in the friction direction, F_2 is the sum of the forces contributed by the opposite side of the particle coating, and f is the internal friction caused by the rotation torque. Fig. 8a–f shows the change in the surface roughness when the coating is worn. Fig. 8a–f are the surface morphology and roughness of ZJ1 best-particles and ZJ2 best-particle coatings at 30%, 50%, and 80% wear rates, respectively. It can be seen that the roughness increases after wear. This is because the particles are also distributed inside the coating and exposed to the surface after wear, so the roughness is improved. These results show that the resin and particles mix well.

3.4 The heat and dust resistance of WSAR/Si–ZrO$_2$–IPDI@OD coating

Fig. 9a–f are thermogravimetric curves of ZJ1 best and ZJ2 best-mixed coatings with different proportions of particles. The

three ratios of 1 : 1, 1 : 5, and 1 : 15 were repeated to confirm that the increase in particle content improved the heat resistance of the coating. The two ratios of 1 : 3 and 1 : 10 were not repeated because their ratios are similar to 1 : 5 or 1 : 15, so it is difficult to obtain clear experimental results. Analysis of the curves in Fig. 9a and d show that there is an obvious trend: more particle content results in a lower loss in the coating quality at high temperatures, because the heat resistance of particles is better than resin. At $T_{10\%}$ (10% weight loss), the 1 : 1 group in Fig. 9a is 10% higher than that in the pure ZJ1 best group, while the 1 : 1 group, as shown in Fig. 9b is 85% higher than that in the pure ZJ2 best group. Combining Fig. 9b, c, e and f, it can be seen that the addition of particles improves the heat resistance of the coating. Fig. 9g shows the change of contact angle with temperature. As shown in the figure, the contact angle of the ZJ2 best-particle coating can be maintained at 300–350 °C. With the temperature increasing above 350 °C, the hydrophobic property is destroyed and the contact angle decreases rapidly. Meanwhile, ZJ1 best-particle coating group has better stability and its contact angle can be maintained at 390 °C. After that, the contact angle drops rapidly. The loss of contact angle is sudden rather than gradual because the hydrophobic groups grafted on
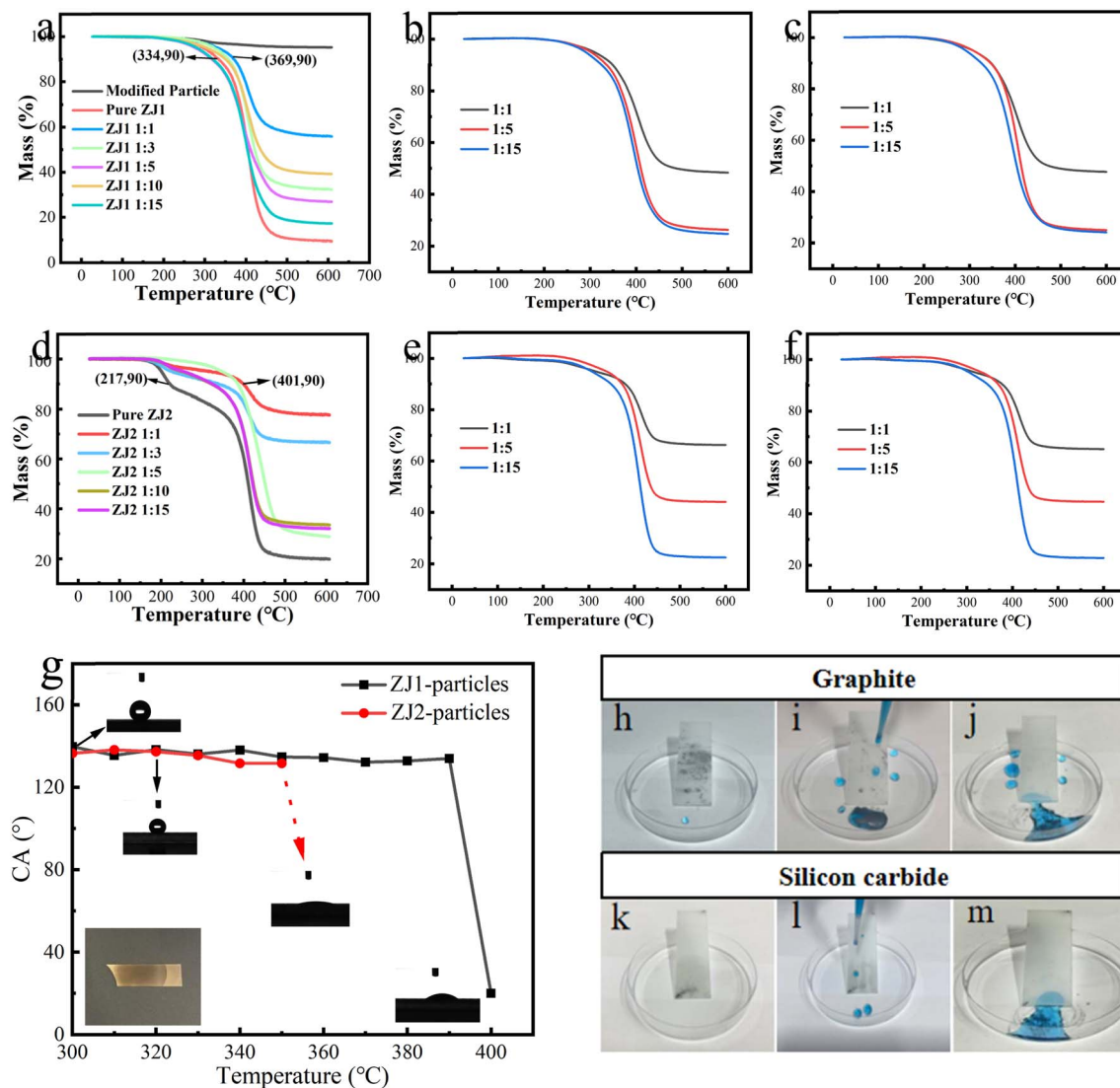
Fig. 9 (a–c) Repeat the experiment of thermogravimetric curves for ZJ1 best-particle coating. (d–f) Repeat the experiment of thermogravimetric curves for ZJ2 best-particle coating. (g) High temperature-contact angle test of two groups of coatings. (h–j) Self-cleaning test of coating stained with graphite particles. (k–m) Self-cleaning test of coating stained with SiC particles.

the surface of ZrO$_2$ particles are burned out, and the ignition point of ZrO$_2$ is about 2700 °C, thus leaving the ZrO$_2$ particles exposed, and its surface will quickly contact water molecules in the air to form a large amount of –OH, so it becomes very hydrophilic. Generally, due to the decomposition of organic molecules at high temperatures, the temperature tolerance range of hydrophobic coatings is often around 350 °C. As mentioned in the introduction, most of the solutions are the introduction of fluorine-containing hydrophobic materials, because the fluoride bond energy is very high and has strong resistance to heat. As widely reported,[50–52] most coatings can withstand 350 °C without a decrease in hydrophobicity, which is close to the ZJ2 best-particles group and lower than that of the ZJ1 best-particles group. Therefore, it also shows that the prepared composite coating has good high-temperature resistance.

The self-cleaning effect of the hydrophobic coating is a very useful property. In this experiment, the self-cleaning ability of the coating on hydrophobic graphite particles and hydrophilic silicon carbide particles was investigated. The coating was first stained with particles, then the stain was removed with blue-dyed water droplets. As shown in Fig. 9(h–j) and (k–m), the self-cleaning performance of the coating is good, and it can be observed that the coating allows water droplets to remove the dirt along the rolling path.

4 Conclusion

We successfully prepared water-based fluorine-free hydrophobic coatings by introducing silanized ZrO$_2$ nanoparticles (Si–ZrO$_2$) into water-based silicon-modified acrylic resin (WSAR) after hydrophobization. The prepared WSAR was optimized by orthogonal experiments, and two preparation schemes were

named ZJ1 best and ZJ2 best. These two composite hydrophobic coatings have a high water contact angle of 141.8° and a low sliding angle of 5° which made the coatings highly self-cleaning. Due to the robust properties of the modified particles and the bonding between the zirconium hydroxyl group on its surface and the silicon hydroxyl group of the resin, the coating exhibited good mechanical and thermal stability. Under the harsh conditions of 20 kPa pressure and 600 mesh sandpaper wear, the wear resistance of the coating was investigated, and the experiment results were fitted and evaluated. The wear resistance of the ZJ1 best-particle coating is better than that of the ZJ2 best-particle coating. This is due to the difference between the synthesis schemes of the ZJ1 best and ZJ2 best. Compared to pure resin, the wear resistance of the coating was greatly improved, up to 150%, and the wear distance reached 45 m while maintaining hydrophobicity. After the wear-contact angle test, the coating could maintain the water contact angle after 70% mass loss. In addition, under optimal conditions, the $T_{10\%}$ of the fluorine-free coating in thermogravimetric experiments was greatly improved compared to the pure resin, reaching 400 °C. Moreover, the water contact angle of the coating could also be maintained after heating at 390 °C.

Conflicts of interest

There are no conflicts to declare.

References

1 L. Feng, S. Li, Y. Li, H. Li, L. Zhang, J. Zhai, Y. Song, B. Liu, L. Jiang and D. Zhu, *Adv. Mater.*, 2002, **14**, 1857–1860.

2 L. Feng, Y. Song, J. Zhai, B. Liu, J. Xu, L. Jiang and D. Zhu, *Angew. Chem., Int. Ed.*, 2003, **42**, 800–802.

3 F. Xia and L. Jiang, *Adv. Mater.*, 2008, **20**, 2842–2858.

4 I. P. Parkin and R. G. Palgrave, *J. Mater. Chem.*, 2005, **15**, 1689–1695.

5 S. Alexander, J. Eastoe, A. M. Lord, F. Guittard and A. R. Barron, *ACS Appl. Mater. Interfaces*, 2016, **8**, 660–666.

6 J. C. Brennan, N. R. Geraldi, R. H. Morris, D. J. Fairhurst, G. McHale and M. I. Newton, *Sci. Rep.*, 2015, **5**, 10267.

7 X. Deng, L. Mammen, H. J. Butt and D. Vollmer, *Science*, 2012, **335**, 67–70.

8 E. Mele, S. Girardo and D. Pisignano, *Langmuir*, 2012, **28**, 5312–5317.

9 J. Carpentier and G. Grundmeier, *Surf. Coat. Technol.*, 2005, **192**, 189–198.

10 V. Stelmashuk, H. Biederman, D. Slavinska, J. Zemek and M. Trchova, *Vacuum*, 2005, **77**, 131–137.

11 T. Soeno, K. Inokuchi and S. Shiratori, *Appl. Surf. Sci.*, 2004, **237**, 539–543.

12 S. Kulinich and M. Farzaneh, *Surf. Sci.*, 2004, **573**, 379–390.

13 G. Zhang, D. Wang, Z.-Z. Gu and H. Möhwald, *Langmuir*, 2005, **21**, 9143–9148.

14 N. Zhao, F. Shi, Z. Wang and X. Zhang, *Langmuir*, 2005, **21**, 4713–4716.

15 H. Liu, L. Feng, J. Zhai, L. Jiang and D. Zhu, *Langmuir*, 2004, **20**, 5659–5661.

16 M. Ma, Y. Mao, M. Gupta, K. K. Gleason and G. C. Rutledge, *Macromolecules*, 2005, **38**, 9742–9748.

17 J. T. Han, Y. Zheng, J. H. Cho, X. Xu and K. Cho, *J. Phys. Chem. B*, 2005, **109**, 20773–20778.

18 M. Hikita, K. Tanaka, T. Nakamura, T. Kajiyama and A. Takahara, *Langmuir*, 2005, **21**, 7299–7302.

19 A. Nakajima, C. Saiki, K. Hashimoto and T. Watanabe, *J. Mater. Sci. Lett.*, 2001, **20**, 1975–1977.

20 D. Wu, S. Z. Wu, Q. D. Chen, Y. L. Zhang, J. Yao, X. Yao, L. G. Niu, J. N. Wang, L. Jiang and H. B. Sun, *Adv. Mater.*, 2011, **23**, 545–549.

21 T. Bharathidasan, T. N. Narayanan, S. Sathyanaryanan and S. S. Sreejakumari, *Carbon*, 2015, **84**, 207–213.

22 X. M. Li, D. Reinhoudt and M. Crego-Calama, *Chem. Soc. Rev.*, 2007, **36**, 1350–1368.

23 L. Boinovich and A. Emelyanenko, *Adv. Colloid Interface Sci.*, 2012, **179–182**, 133–141.

24 L. Wen, Y. Tian and L. Jiang, *Angew. Chem., Int. Ed. Engl.*, 2015, **54**, 3387–3399.

25 Y. Lu, S. Sathasivam, J. Song, C. R. Crick, C. J. Carmalt and I. P. Parkin, *Science*, 2015, **347**, 1132–1135.

26 I. Bayer, *Coatings*, 2017, **7**, 12.

27 A. Esmaeilirad, M. V. Rukosuyev, M. B. G. Jun and F. C. J. M. van Veggel, *Surf. Coat. Technol.*, 2016, **285**, 227–234.

28 M. Ochi, D. Nii, Y. Suzuki and M. Harada, *J. Mater. Sci.*, 2010, **45**, 2655–2661.

29 A. Steele, A. Davis, J. Kim, E. Loth and I. S. Bayer, *ACS Appl. Mater. Interfaces*, 2015, **7**, 12695–12701.

30 F. Zhao, J. Guan, W. Bai, T. Gu and S. Liao, *Prog. Org. Coat.*, 2019, **131**, 357–363.

31 B. Wang, T. Qian, Q. Zhang, X. Zhan and F. Chen, *Surf. Coat. Technol.*, 2016, **304**, 31–39.

32 E. D. Şam, S. Kirtay and V. Gunay, *Key Eng. Mater.*, 2004, **264–268**, 379–382.

33 H. Ye, L. Zhu, W. Li, H. Liu and H. Chen, *J. Mater. Chem. A*, 2017, **5**, 9882–9890.

34 J. Armitage, I. T. Cousins, R. C. Buck, K. Prevedouros, M. H. Russell, M. MacLeod and S. H. Korzeniowski, *Environ. Sci. Technol.*, 2006, **40**, 6969–6975.

35 D. A. Ellis, S. A. Mabury, J. W. Martin and D. C. Muir, *Nature*, 2001, **412**, 321–324.

36 C. Lau, J. L. Butenhoff and J. M. Rogers, *Toxicol. Appl. Pharmacol.*, 2004, **198**, 231–241.

37 E. Besson, A.-M. Gue, J. Sudor, H. Korri-Youssoufi, N. Jaffrezic and J. Tardy, *Langmuir*, 2006, **22**, 8346–8352.

38 H. Jin, X. Tian, O. Ikkala and R. H. Ras, *ACS Appl. Mater. Interfaces*, 2013, **5**, 485–488.

39 H. Liu, L. Feng, J. Zhai, L. Jiang and D. Zhu, *Langmuir*, 2004, **20**, 5659–5661.

40 Y. Li, S. Chen, M. Wu and J. Sun, *Adv. Mater.*, 2014, **26**, 3344–3348.

41 X. Zhang, H. Wang, X. Zhang, Z. Zhao and Y. Zhu, *Colloids Surf., A*, 2019, **568**, 239–247.

42 S. Xiao, X. Hao, Y. Yang, L. Li, N. He and H. Li, *Appl. Surf. Sci.*, 2019, **463**, 923–930.

43 F. Su and K. Yao, *ACS Appl. Mater. Interfaces*, 2014, **6**, 8762–8770.

44 W. Ma, Z. Yang, M. B. Asif, Y. Zhang, W. Li, J. Yang and S. Yao, *ACS Appl. Eng. Mater.*, 2023, **1**, 519–529.

45 H. P. Wang, M. J. He, H. Liu and Y. C. Guan, *ACS Appl. Mater. Interfaces*, 2019, **11**, 25586–25594.

46 G. W. Stachowiak and A. W. Batchelor, *Engineering tribology*, Butterworth-heinemann, 2013.

47 L. Chang and K. Friedrich, *Tribol. Int.*, 2010, **43**, 2355–2364.

48 L. Chang, Z. Zhang, L. Ye and K. Friedrich, *Wear*, 2007, **262**, 699–706.

49 Z. Zhang, C. Breidt, L. Chang, F. Haupert and K. Friedrich, *Composites, Part A*, 2004, **35**, 1385–1392.

50 L. Li, T. Huang, J. Lei, J. He, L. Qu, P. Huang, W. Zhou, N. Li and F. Pan, *ACS Appl. Mater. Interfaces*, 2015, **7**, 1449–1457.

51 W. Chen, W. Wang, D. X. Luong, J. T. Li, V. Granja, P. A. Advincula, C. Ge, Y. Chyan, K. Yang, W. A. Algozeeb, C. F. Higgs 3rd and J. M. Tour, *ACS Appl. Mater. Interfaces*, 2022, **14**, 35053–35063.

52 T. Yang, M. Wang, X. Wang, X. Di, C. Wang and Y. Li, *Soft Matter*, 2020, **16**, 3678–3685.